

Statistical Review of Tsunami Generated by Earthquake-Produced Submarine Landslides and Tsunami Direct Path GIS Impact Analysis

John E.S. Saunders

Abstract

This research exclusively uses Geographic Information Systems (GIS) to analyze the potential for, and impacts of, catastrophic tsunami generated along the eastern North American continental shelf by submarine mass failures (SMF, also known as submarine landslides). It uses a multiphase approach that includes examining earthquake data in the eastern United States, analyzing topographic bathymetry within the mid-Atlantic shelf and slope, anticipating the propagation of a potential tsunami surface wave, and developing a hypothetical impact analysis on the first populated coastal area within the surface wave's path. The study considers key variables and thresholds for tsunami generation, including but not restricted to location of seismic events, relative epicenter depth and magnitude, and seafloor topography and layout, to determine which areas are prone to failure as a consequence of a catalyst seismic event. It also features an analysis of key demographic, lifeline, infrastructure, and economic impacts on an area likely to be affected by a potential tsunami. The final product brings attention to seismically active regions of the United States East Coast susceptible to tsunami threat.

Table of Contents

INTRODUCTION	1
RESEARCH PHASES	2
PHASE 1 – EARTHQUAKE AND TSUNAMI STATISTICAL DATA ANALYSIS	3
<i>The Currituck Submarine Mass Failure</i>	3
<i>Statistical Analysis of Earthquake Event Data</i>	6
PHASE 2 – SEAFLOOR ANALYSIS	11
<i>Site Selection</i>	14
PHASE 3 – TSUNAMI WAVE PROPAGATION MODELING	19
<i>GIS Least Cost and Buffer Method for Wave Impact Location Identification</i>	19
<i>Tsunami Inundation Impact Model</i>	22
PHASE 4 – WAVE INUNDATION IMPACT ANALYSIS	24
<i>Results</i>	27
CONCLUSIONS	31
REFERENCES	33

List of Figures

FIGURE 1. OUTER CONTINENTAL SHELF (OFFICE OF NAVAL RESEARCH, USG).	4
FIGURE 2. INTERPRETIVE GENERAL SCHEMATIC DRAWING OF THE CURRITUCK SLIDE.	5
FIGURE 3. BREAKDOWN OF TOTAL EARTHQUAKE EVENTS BY MAGNITUDE.....	7
FIGURE 4. 612 TOTAL EARTHQUAKE CENTROID EPICENTERS AND DATA FILTERING.....	8
FIGURE 5. 95 TOTAL EARTHQUAKE CENTROID EPICENTERS AND DATA FILTERING	9
FIGURE 6. 100 KM BUFFER FROM U.S. EAST COAST CONTAINING 17 EARTHQUAKE EVENTS.....	10
FIGURE 7. TOTAL EARTHQUAKE EVENTS ALONG UNITED STATES EAST COAST STATES	11
FIGURE 8. BATHYMETRY AROUND THE CURRITUCK SMF SITE.....	13
FIGURE 9. DISTRIBUTION OF CONTINENTAL SHELF LAYERS AND SLOPE ANALYSIS OF THE INNER AND MID CONTINENTAL SHELF	15
FIGURE 10. SOUTHEAST DEPTH MODEL FOR CANDIDATE RESEARCH LOCATION IDENTIFICATION	17
FIGURE 11. SOUTHEAST SLOPE MODEL FOR CANDIDATE RESEARCH LOCATION IDENTIFICATION	18
FIGURE 12. RANGE RINGS IDENTIFY IMPACT LOCATION,.....	20
FIGURE 13. RECLASSIFIED SLOPE ANALYSIS BY COST.....	21
FIGURE 14. REPRESENTATION OF WAVE IMPACT ON ISLE OF PALMS.....	23
FIGURE 15. CLACK MODEL SCRIPT USER INTERFACE	24
FIGURE 16. CLACK MODEL INPUT LAYERS.....	25
FIGURE 17. DEM TO MULTIPOINT	25
FIGURE 18. HYDROLOGY RASTER TO TIN.....	26
FIGURE 19. SNAPPED TIN TO RASTER.	26
FIGURE 20. DIFFERENCE MODEL.....	28
FIGURE 21. CLACK HYDROLOGY FLOOD MODEL.....	29
FIGURE 22. SITE-SPECIFIC INUNDATION LOCATIONS.....	30

Introduction

Tsunami have the potential to cause catastrophic loss of life because there is often little information available to population centers most likely to be affected by these natural hazards. Globally, loss of life from tsunami in the past ten years totals over 250,000 people (USGS, 2014). Efforts such as the work proposed here will provide new planning tools and methods to help scientists and practitioners better understand how geography can play an important role in predicting and preparing for tsunami, thereby reducing their impact on human life and society.

Tsunami produced by a submarine landslide appear to be important to the U.S. East Coast. Recent computer simulations of deep-water Submarine Mass Failures (SMFs), using the North Goringe Avalanche characteristics as the model, illustrate the potential of wave amplitudes greater than 15 meters (Iacono et al., 2012). Submarine volcanoes and volcanic islands, where an entire flank of a volcano can collapse, also pose a large threat and could result in a mega-tsunami. For example, the Cumbre Vieja volcano in the Canary Islands has the potential to suffer a major flank collapse and poses a major threat to near-field and far-field¹ coastal regions in North America, Western Europe, and West Africa (Harris et al., 2012).

Little information is known about tsunami triggered by submarine landslides, which – in addition to potential loss of human life – can result in significant damage to material assets such as underwater telecommunication lines, coastal city infrastructure, agriculture plots, and power plants. There are numerous ways to identify this threat (Bardet et al., 2003). Among these means, recognizing the physical conditions conducive to producing large submarine landslides is an important topic in determining the probability of their occurring (Harbitz et al., 2014).

Understanding the above-surface and submarine topography and geology where these and other forms of landslides are generated is essential in determining the approximate wave height generated by the displacement of water. Metadata such as the duration, depth, slope angle, and the distance traveled by the sliding mass all contribute to the effects of the landslide (Sammarco and Renzi, 2008; Heiarzadeh et al., 2015). Attention to shallow- and deep-water landslides is important. Studying the seafloor makeup from the perspective of rock/soil composition can also be useful in identifying areas with large amounts of clay deposits, which provide a slick surface area for rock masses to slide on and consequently increase the range of motion or decrease the tolerance levels for (L'Heureux et al., 2013).

¹ Near-field tsunami are those with waves capable of reaching land in less than 30 minutes of generation. Mid-field tsunami are those that strike land between 30 minutes and 2 hours after generation. Far-field tsunami are those that strike land after more than 2 hours after generation (<http://nthmp-history.pmel.noaa.gov/terms.html>).

In contrast to SMFs, tsunami triggered by earthquakes at subduction zones are less likely along the U.S. East Coast but are the more likely source of large tsunami worldwide. Several numerical equations exist to help in calculating the sea surface wave height and propagation created by the displacement of water associated with tsunami generation. Using analytical approaches in determining the amplitude of the wave-height can reveal the likelihood of the wave breaking (Tinti and Tonini, 2005). Although primarily applied to tsunami generated by earthquakes at subduction zones, these equations are used to help build models based on the displacement resulting from the seismic events and associated landslides. Boussinesq Equations are the principal means of addressing nonlinear tsunami propagation and generation (Zhao et al., 2009). In the present study, these equations will be examined to determine their utility for implementation in a Geographic Information System (GIS) or statistical software tool.

In addition to the topography of the terrain features surrounding earthquake- and landslide-induced tsunami, the distance of near- and far-field effects of either event is a key factor when determining the potential impact of a tsunami on coastal regions. It is also important to consider that both long waves associated with earthquakes and short waves associated with SMFs are susceptible to attenuation as a factor of ocean depth and the distance to the sea surface (Grilli et al, 2012). Furthermore, to assist in determining the tsunami run-up, the achievable velocity and amplitude are calculated to define how each is affected by the transition, breaking, and non-breaking of a tsunami when it encounters variable water depths on a slope (Park et al., 2015).

This project will to some degree build upon the literature reviewed above and especially on the work of Grilli et al. (2015), who modeled SMF activity in the North Atlantic Ocean and developed an impact analysis for a tsunami striking Ocean City, MD. My project will expand that effort geographically by studying multiple exposed locations along the U.S. East Coast and, at the same time, look more closely at the potential impacts that vulnerable areas exposed to a tsunami could undergo. The following section systematically presents the research in more detail.

Research Phases

This research uses a four-phase approach to assess the risk and potential impacts of SMF-induced tsunami along the U.S. East Coast. Phase 1 involves examining earthquake data in the eastern United States, whereas Phase 2 comprises analyzing topographic bathymetry along the mid-Atlantic shelf and slope. Phase 3 anticipates the propagation of a potential tsunami surface wave, and Phase 4 develops an impact analysis for a hypothetical SMF-generated tsunami that strikes a populated coastal area.

To accomplish this, all work was completed using a 2012 MacBook Pro Retina 16GB partitioned to Windows 7. Software used for the entirety of the analysis included ESRI ArcGIS 10.3, ArcScene, ESRI City Engine Web Viewer, QGIS 2.2 Valmiera, R, Google Sketch-up Pro, and the MITRE ISR Forensics Tool.

Phase 1 – Earthquake and Tsunami Statistical Data Analysis

Phase 1 investigated the most pronounced Atlantic SMF, the historic Currituck submarine landslide, which produced a moderate tsunami triggered by the failure of an approximately 20 km wide rigid slump on the North American continental slope (Locat et al., 2008), to obtain control data. These control data were then used as the basis for Phase 2 when searching for a candidate location along the East Coast. After studying the Currituck event, a statistical analysis of earthquake event data associated with historical tsunami was conducted. The findings were used to assist a statistical and spatial analysis of seismic events near the U.S. East Coast. That analysis aimed at identifying hot spots and event clusters in the vicinity of a susceptible submarine rigid slump or of any area that met the control parameters for an SMF or landslide.²

The Currituck Submarine Mass Failure

The Currituck SMF took place somewhere between 24,000–50,000 years ago (Locat et al., 2008) on the North American continental slope off the coast of what is now Virginia Beach, Virginia. Many scholarly articles and papers have been written about the Currituck SMF (e.g., Prior et al., 1986; Locat et al., 2008; and Grilli et al., 2015), but the description here focuses only on the main variables needed to construct the pre-failure ocean bathymetry and on the characteristics of the surface wave produced by the event. Emerging from this description are the control data points used in the current study as the basis of the hypothetical tsunami surface wave.

To understand the characteristics of an SMF or landslide, it is important to comprehend the structure of the East Coast seafloor itself. Five components are involved: the coast, continental shelf, continental slope, continental rise, and ocean floor (Figure 1; Office of Naval Research, USG).

² The following methods for researching seismic activity only through spatial and statistical analysis are based on a research paper titled, *Spatial Analytical Review of Coastal Japanese Earthquakes*, produced for GEOG 586 in Summer II 2015.

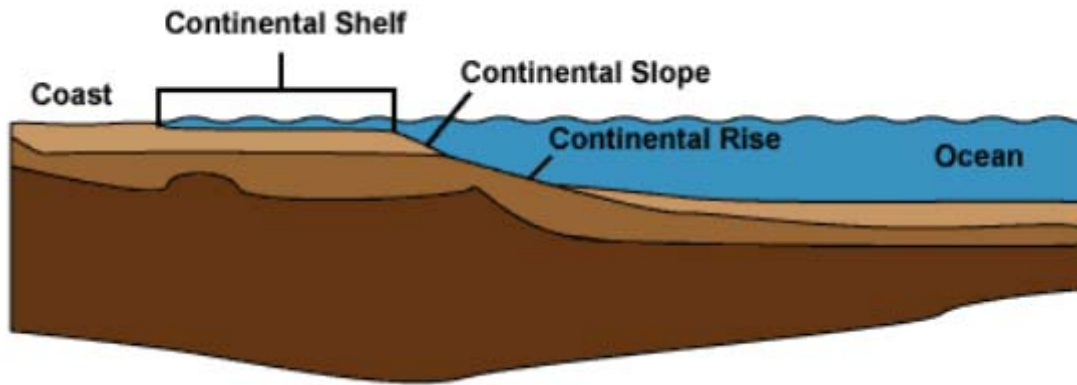


Figure 1. Outer continental shelf (Office of Naval Research, USG).

Leading up to the break in slope denoting the top of the continental slope is the continental shelf, a very low-gradient slope extending from sea level along the shoreline to approximately 100 m below sea level at the continental slope ridgeline. Here, the slope gradient becomes steep and ideal for landslides. The Currituck SMF is believed to have been located along the break in slope at least at two locations over the span of 20 km (Grilli et al., 2015), with the initial failure taking place at 36.39N, 74.61W.

Geomorphological analysis, primarily conducted by Prior et al. (1986) and based on high-resolution multibeam data, indicates that before the slide, the upper (slide 1) escarpment had an angular slope of 9° - 10° and the lower (slide 2) escarpment had an angular slope of 15° - 30° . These lower slope angles are not unusual in submarine landslides because the angle of repose can have very small values in saturated clays and sands, enabling the materials to flow more like a fluid than tumble like a landslide once it is set in motion (Mehta and Barker, 1994). An estimated 128 km^3 of sediment are calculated to have been displaced by the slide (Prior et al., 1986). Post failure, the upper escarpment was replaced by an upper scarp calculated at 12° followed by a 4° floor, and the lower scarp now had a slope angle of 12° with a residual trough floor of 1° (Prior et al., 1986; see Figure 2).

The final aspects of the Currituck SMF, which needed to be investigated, are surface wave characteristics created by the tsunamigenic sub-surface wave that describes the initial energy released. This energy translates to the instantaneous vertical amplitude at nadir of the failure and then the amplitude of the surface wave itself over the distance to coastal land areas.

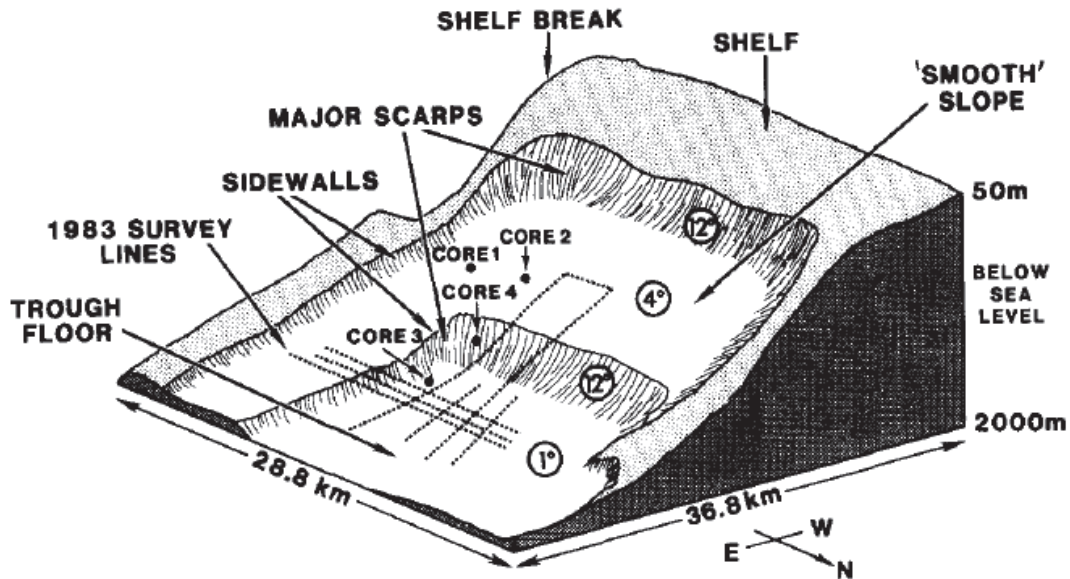


Figure 2. Interpretive general schematic drawing of the Currituck slide showing major morphological components (Prior et al., 1986).

SMF modeling work carried out by Grill and Watts (1999, 2005), Grilli et al. (2002), Lynette and Lieu (2002, 2005), and Watts et al. (2005) found that “besides the volume and mean submergence depth,” the primary catalyst for tsunami creation is the initial acceleration on the downward slope placing the largest emphasis on rigid slumps also known as rotational slides (Grilli et al., 2015), where the surface of rupture is curved concavely upward and the slide movement is roughly rotational about an axis that is parallel to the ground surface and transverse across the slide (USGS, 2004).

Typically, when modeling an SMF, a non-hydrostatic model NHWAVE (NHW) equation is used, which uses a coordinate grid in the vertical direction, a Cartesian horizontal grid linearly, and is effective for 3D modeling. Once SMF motion halts, surface elevation and horizontal velocity are then “interpolated into the non-linear and dispersive lone-wave Boussinesq model FUNWAVE-TVD (FNW)”¹, which is normally used to evaluate wave propagation to coastal areas and more appropriate in 2D modeling (Ma et al., 2012) (Grilli et al., 2015)¹. During the Currituck slide once all tsunamigenic motion had ceased approximately 710 seconds after the initial acceleration, instantaneous surface waves were calculated at amplitudes of 40 meters (-20 and +20). As Grilli et al., (2015) explains, the actual wave that will propagate onshore is referred to as the “initial negative elevation wave,” which will propagate in the opposite direction of the rotational slide. It is furthered reinforced by a “rebound wave” from the crest of the of the peak amplitude. These two waves, referred to as an N-wave, will propagate towards coasts. Other waves that are generated offshore still result in refraction on other parts of the continental shelf and re-orient towards other coastal locations.

The waves began to attenuate as bottom friction of more shoal waters was encountered, directional spreading continued, and as waves began to break. The resulting waves that made landfall in the Virginia Beach vicinity did so with a maximum surface elevation of 3–6 meters (Grilli et al., 2015).

Statistical Analysis of Earthquake Event Data

A span of time covering the period from 1 January 1990–January 2015 was used as the range of earthquake events to be examined. This date range is abstract as many seismic events take place each year. Also, due to the fact that mega-earthquakes tend to take place over the course of thousands of years, adding more average datasets would most likely not affect the outcome. Buffers were used to extract data at a distance of 100 km from the eastern coastline because of the unlikelihood of seismic data beyond that limit having an effect on submarine candidate sites.

Results for the most probable coastal region containing the highest volume of seismic events was anticipated to lie within the northeastern United States. It was further anticipated that the hotpot with the highest number of events would not be the same locale where the greatest magnitude seismic events took place in the period of research. This hypothesis is based on assumption that many smaller events happening at a seismically active location will tend to relieve stress, whereas larger earthquakes will tend to occur in areas that have not experienced a seismic shift in a greater amount of time thereby allowing stress to build.³

Point data for the east coast of the United States was collected using the United States Geologic Survey (USGS) Earthquake Hazards Program web tool (<http://earthquake.usgs.gov/earthquakes/search/>). Data were selected between January 1990 and January 2015 for all levels of earthquake magnitudes recorded. This metric encompassed magnitudes ranging 1.0–10.0 and was geographically covered a 300km buffer centered on the U.S. east coast. See Figure 2 for the total collected points in the research period and the initial step in filtering data. Stemming from previous research on the lower threshold limits regarding earthquakes produced by subduction zones, which are likely to generate tsunami, a limit was initially placed on the data where all centroid epicenter earthquake locations less than 3.0 were disqualified for research. In exclusive earthquake-produced tsunamis, an average of 7.0–7.5 magnitude event is needed (Parry, 2011). As an example, the 2011 Tohoku, Japan earthquake was measured at 9.0 while the 2004 Indian Ocean (Indonesia) earthquake measured 9.1 (USGS Earthquake Hazards Program). Both events manifested massive tsunami that cost thousands of lives. Since the dataset, which included 612 individual events, had a minimum of 1.0 and maximum of 5.8, still far below the normal criteria for generating an exclusive earthquake produced tsunami, limiting the research to 3.0 seemed appropriate. Of the original 612 data points, only 95 or 16% had magnitudes greater than or equal to 3.0. See Figure 3 for a graphical representation of the proportion of those data points between 3.0–5.8 and Figure 4 for a comparison of location of events.

³ The following methods for researching seismic activity only through spatial and statistical analysis is based on a research paper titled, *Spatial Analytical Review of Coastal Japanese Earthquakes*, produced for GEOG 586 in Summer II 2015.

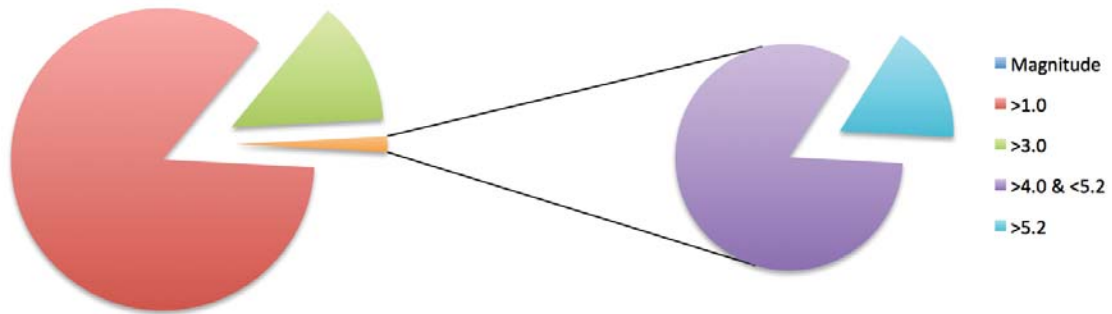


Figure 3. Breakdown of total earthquake events by magnitude.

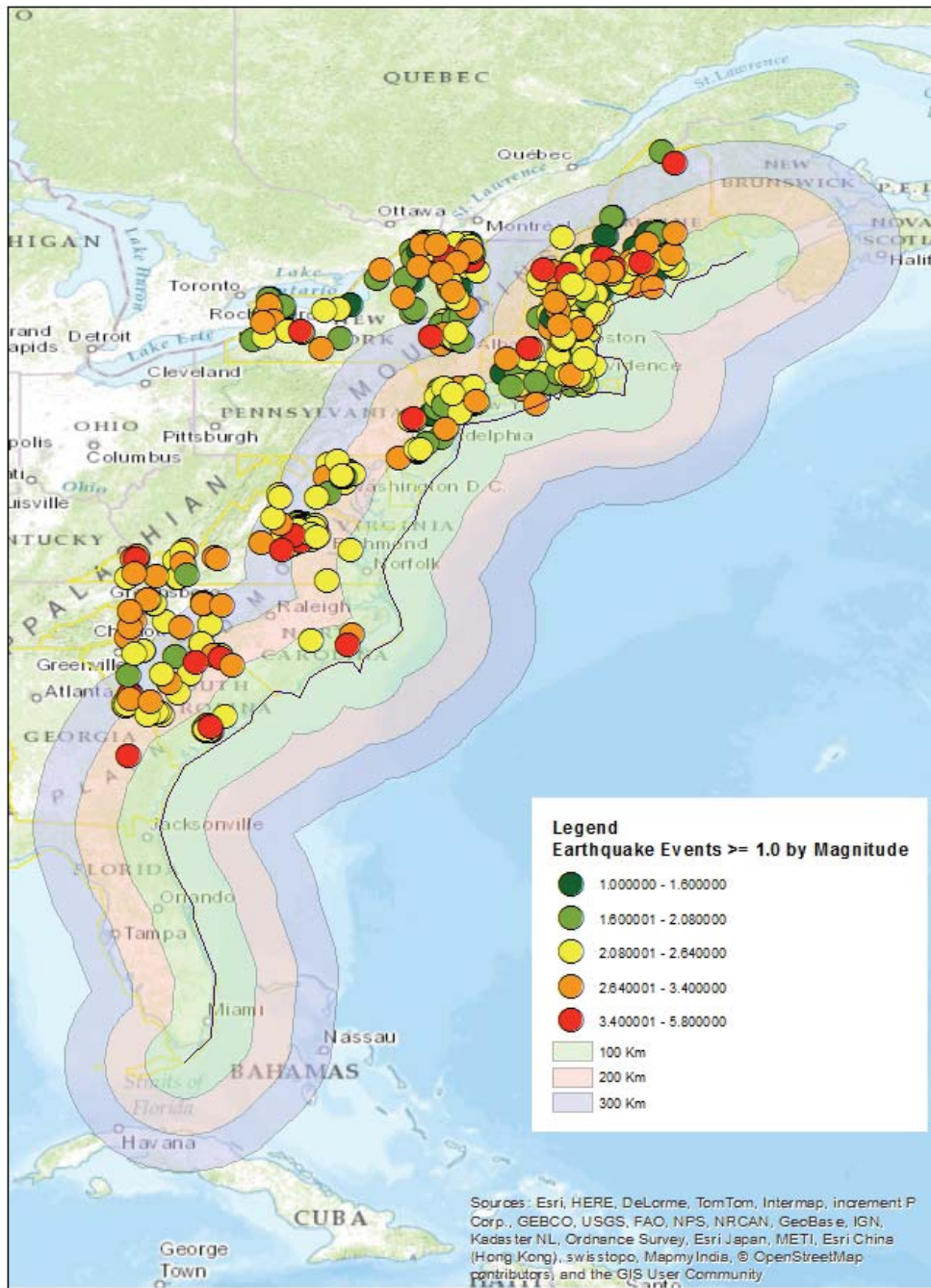


Figure 4. 612 Total earthquake centroid epicenters and data filtering by magnitude > 1.0 .

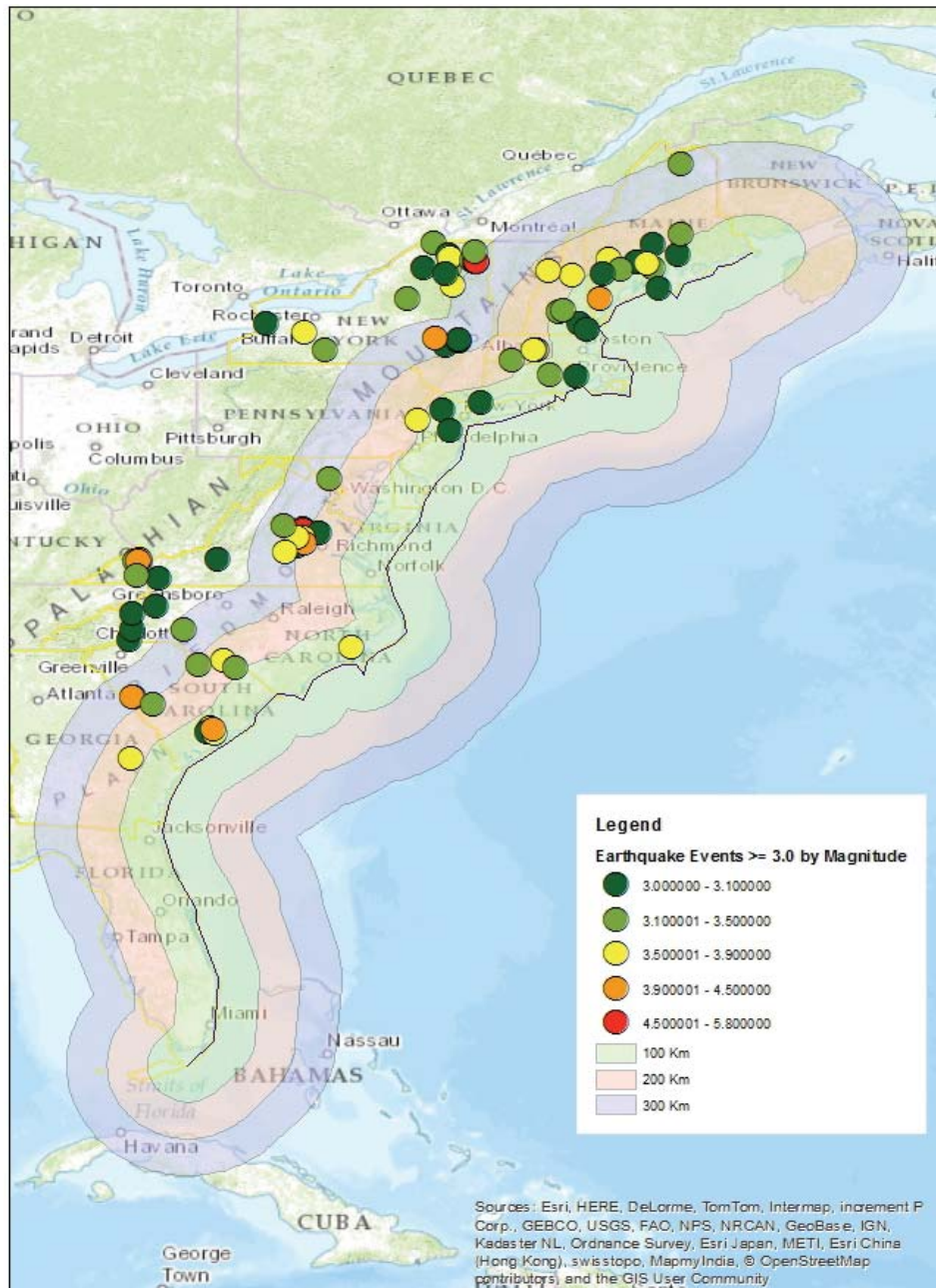


Figure 5. 95 Total earthquake centroid epicenters and data filtering by magnitude > 3.0.

After data were thinned by eliminating data less than the magnitude 3.0 threshold (Figure 5), further earthquake data points were eliminated because – given their magnitudes – their locations were too far inland to trigger an SMF along the continental slope. For this reason, a 100 km buffer was chosen to extract those data closest to the coastal areas (Figure 6). Just 17 earthquake events, or 3% of the original dataset, remained after the clipping, primarily located in New England and in the vicinity of Charleston, South Carolina.

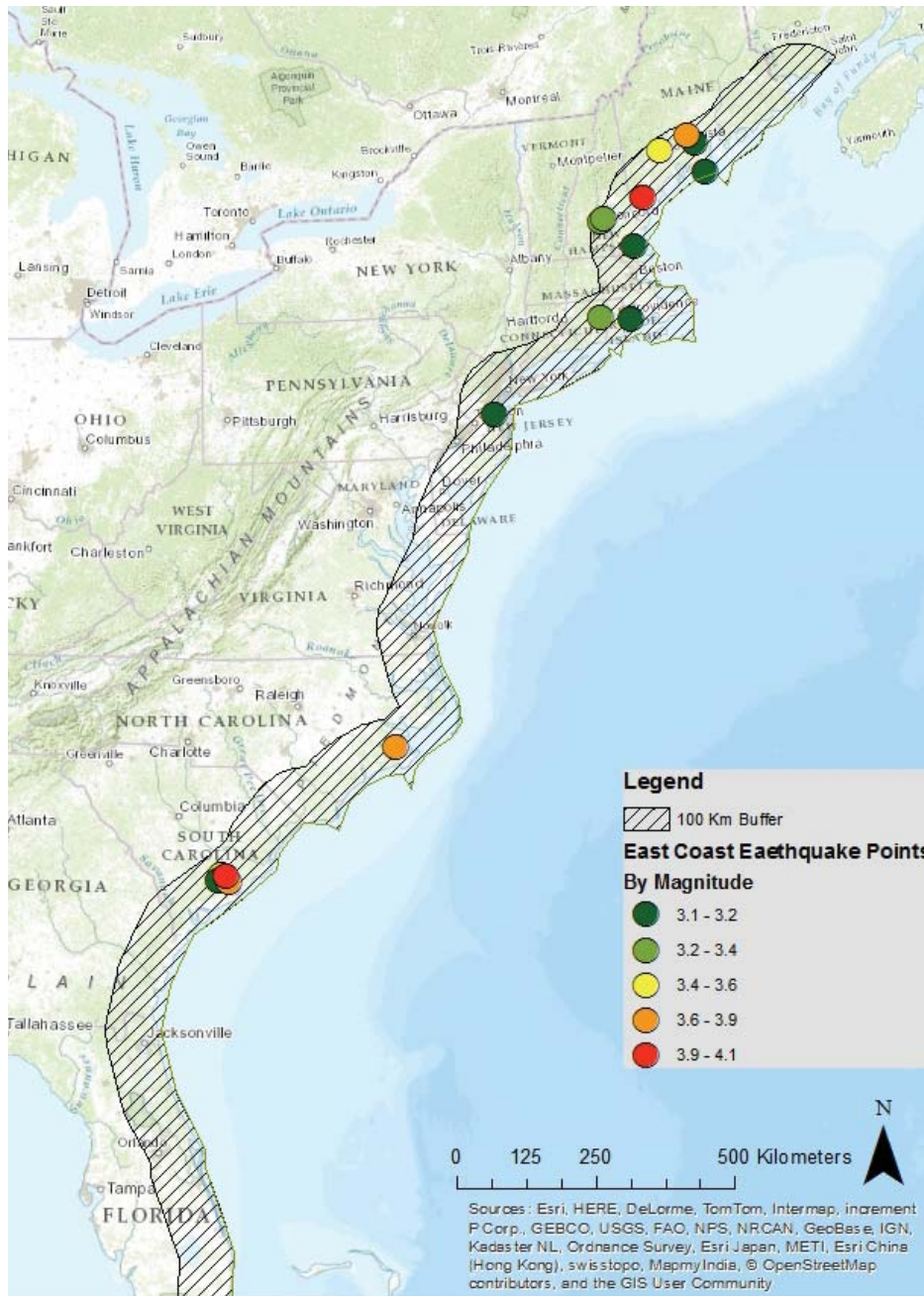


Figure 6. 100 km buffer from U.S. East Coast containing 17 earthquake events.

Kernel Density Estimation (KDE) analysis was used to help both visualize and aggregate the areas with the greatest volume of events in the most exclusive regions. R, an open-source statistical software application, was used to plot KDE maps. Figure 7 depicts all earthquakes measuring 3.0 and greater on the left and then those measuring 3.0 and greater and within 100 km of the coast on the right. Both maps use a bandwidth factor of 1.0, a value calculated within R based on the distribution of points, due to the discreteness of the datasets caused by having too few events. Although more earthquakes (10 events) took place in the New England region, the data are too dispersed across a

large area to pin-point any one location as being seismically active. In contrast, the data for the 5 events experienced in the Charleston area are centric to the city and its limits (5 events).

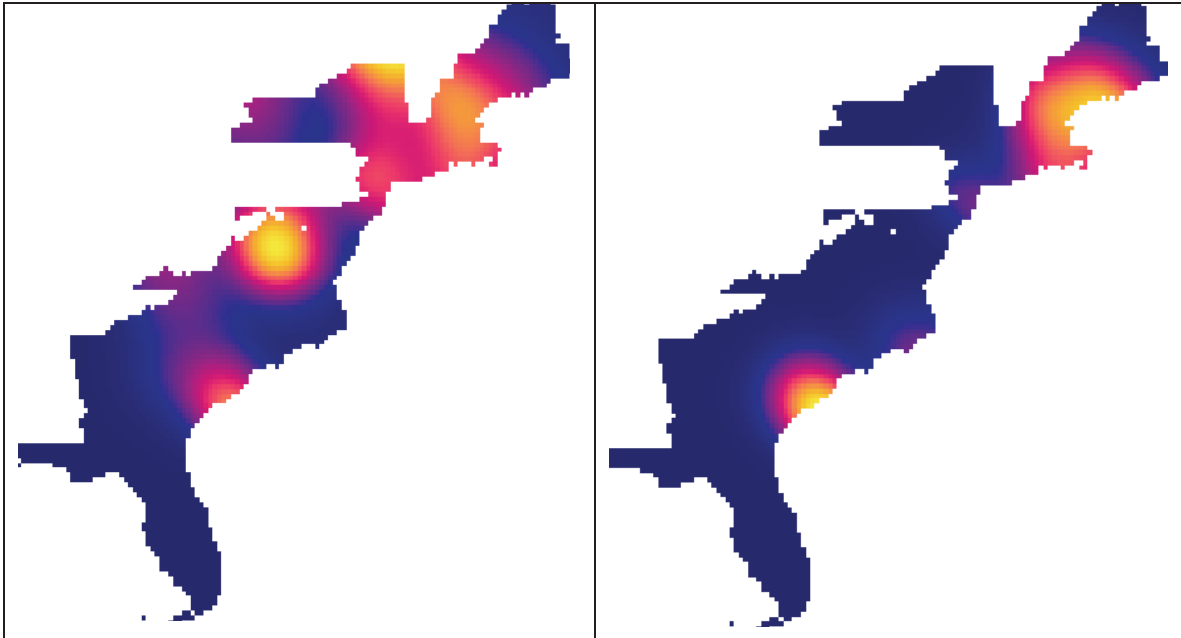


Figure 7. Total earthquake events along U.S. East Coast states (left), research data based on 100 km from U.S. East Coast; (right). Dataset covers a period from Jan 1990–Jan 2015.

Phase 2 – Seafloor Analysis

Phase 2 used bathymetric data to perform a slope analysis of the seafloor within the near-field. The purpose of this analysis was to characterize the submarine topography in an effort to (1) identify a candidate location most similar to the Currituck SMF control scenario, (2) determine the characteristics of a potential failure in order to predict wave amplitude as a surface wave, (3) ascertain where attenuation of the waves' amplitude would be minimally affected, and (4) pinpoint the first human coastal habitat within the tsunami wake.

Bathymetric data obtained from the National Center for Environmental Information, a department within the National Oceanic Atmospheric Administration (NOAA), were used to model the seafloor by constructing a digital elevation model (DEM) for the southeastern portions of the North American continental shelf and slope where available. The imagery was downloaded as 3 arcsecond or 87 m resolution ASCII files and then converted to GeoTIFF within ESRI ArcGIS 10.3. The entirety of the Southeast Atlantic Coast relief model was obtained, which covered coastal state regions from southern New Jersey to northern Georgia. Multibeam bathymetric data were available at higher resolution, as good as 1/3 arcsecond, 10 m resolution, but were extremely limited in the areas that they covered. Most were in support of hurricane inundation forecasting around

major cities such as Virginia Beach, Virginia and Myrtle Beach, South Carolina. These specialized areas also did not adequately extend to areas where potential landslides exist along the continental ridge and slope. Due to the size of the DEM and the amount of computing resources necessary to run otherwise simple tool functions, areas that were not in the vicinity of any land-based seismic activity were extracted from the scene and removed. After the extraction, southern North Carolina became the northern limit for the study area.

A degree slope analysis was then performed using the DEM, in which each pixel of the output raster was classified by its neighbor pixels to identify the steepness between them for a range of 0° to 90° (ESRI, 2007). Initial slope analysis on the relief model produced unanticipated results based on the parameters surrounding the Currituck slide. Understanding the degree of slope was important for finding submarine regions that most closely achieved an angle of repose of 30°, as previously discussed regarding the lower escarpment of the Currituck slide. Also knowing the overall slope of the continental shelf rising up to the coast and the water depth of the seafloor was important for determining the attenuation effects that the sea depth had on surface wave potential energy. This will be discussed further when describing the methods used for calculating the least-cost path of the tsunami propagation from the candidate SMF location to the coast.

Because of the cluster of seismic activity around Charleston SC, based on proximity, the continental shelf to the east of South Carolina was chosen as the most probable location for a landslide to occur. As previously discussed, the control data for this analysis was based upon characteristics of the pre- and post-failure Currituck SMF landslide deposits. Prior et al. (1986) calculated the pre-failure slope to between 9° to 10° and 15° to 30° for the top and bottom of the escarpment, respectively. However, a method was needed to evaluate the post-failure slope of the present day Currituck slope in order to test potential candidate locations in the research area. To that end, Figure 8 shows a top-down view of the pre- and post-failure Currituck SMF deposits. Grilli et al. (2015) calculated the post-failure slope bathymetry at approximately 4°. Using a matrix of linear distances coupled with sea depths, each depth change over distance was converted to rise over run in meters. The arctangent equation was then applied to calculate each change over distance from a perspective of slope (in radians and then converted to degrees).⁴

$$\theta = \arctan\left(\frac{\textit{opposite}}{\textit{adjacent}}\right) = \arctan\left(\frac{\textit{rise}}{\textit{run}}\right) = \chi^\circ$$

All resulting angles were averaged and found to equal a downward slope of 4° to 6° when a variety of measurements were calculated based on the Figure 8 model.

⁴ <http://www.excelfunctions.net/Excel-Atan-Function.html>

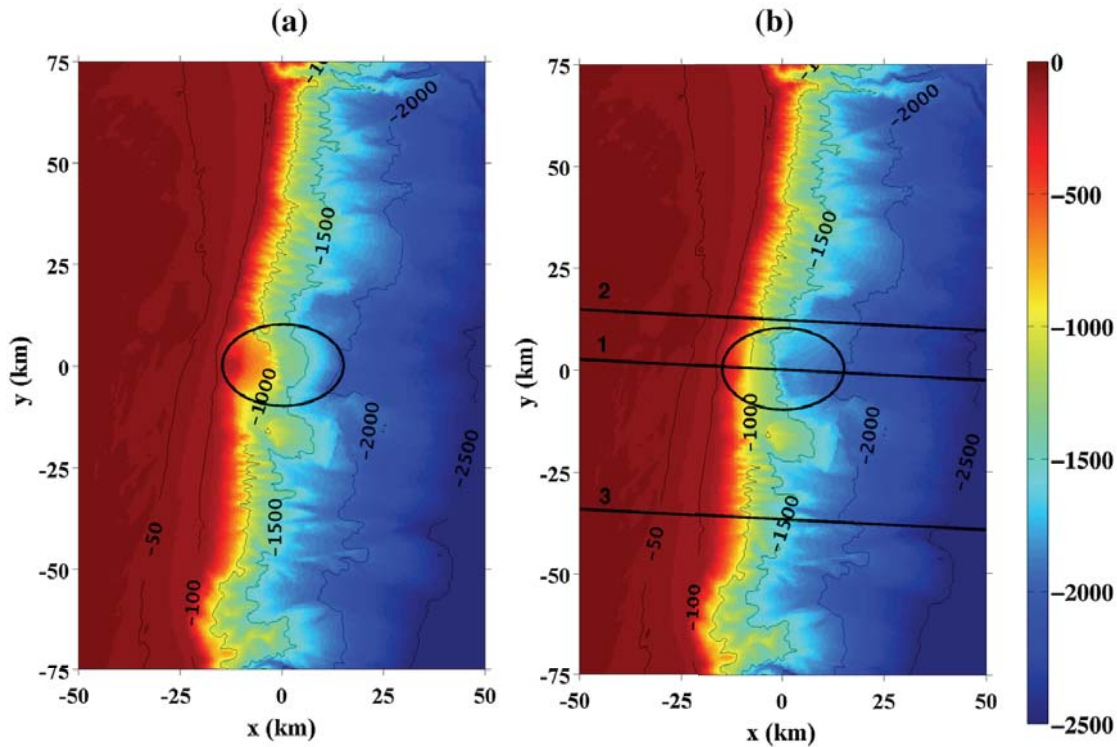


Figure 8. Bathymetry around the Currituck SMF site. “Color scale and bathymetric contours give depth in meters. The ellipse is the SMF footprint and axes mark the distance measured from the SMF center (at 74.61W, 36.39N): a reconstructed (pre-failed) bathymetry; b current (post-failed) bathymetry with black lines marking bathymetric transects. The Currituck SMF central axis corresponds to transect 1” (Grilli et al., 2015).

Initial results of the slope analysis were puzzling as the map indicated almost no distinction for most of the shelf, only showing changes no greater than 10° at the easternmost edge. Maintaining a resolution of 87 m, the analysis was performed multiple times to ensure output continuity and the data were inspected for errors. When no data issues were discovered, closer investigation of the southeastern U.S. continental shelf revealed that as one moves south from southeastern Virginia, the continental shelf resolves into three zones: the inner, mid, and outer shelves. These three zones exist for the entirety of the shelf, but are far less separated to the north and therefore difficult to distinguish in the vicinity of the Currituck SMF. The available imagery data did not include areas beyond the inner shelf and part of the mid shelf, so the slope angles are very small. The steepest locations were those where the transition begins from the inner to mid shelf. Figure 9 displays the portion of the shelf covered by the slope analysis. Since high-resolution multibeam imagery is not widely available except for discrete regions of the shelf, the southeastern inner and mid shelf – and not the steeper outer shelf and continental slope– would have to be used for the duration of the research.

It is worth noting that the same resolution dataset available for the northeastern U.S. showed much steeper slopes ranging upwards of 20° at the outer shelf and even steeper slope angles within canyons. Distances between seismic locations and the outer shelf are much longer, ranging 350–450 km from the most seismically active regions of Maine. However, despite the favorable submarine topography in the Northeast, because available

bathymetric imagery for the Southeast only covers the inner and mid shelves, it is not possible to verify the potential for landslides along the region's outer shelf and continental slope.

Site Selection

Three sections of the research area were examined to isolate the candidate location that would serve as the epicenter for potential landslides and resulting tsunami. It is important again to recognize imagery data inconsistencies that existed in the relief model that included wide swaths of terrain missing between portions of the mid shelf descent. Information could not be found to understand this gap in bathymetric coverage. All further analysis and conclusions acknowledge this discrepancy and focus on the data that are available.

As seen in Figure 10, the southernmost region, Candidate Site 3, exhibits the most consistent ridges, but the descent depth from the ridges themselves is too small to allow a landslide to gain acceleration, dropping approximately 100 m from the steepest point. The northernmost Candidate Site 2, located east of Wilmington, North Carolina, shows more promise in having greater differences in depths, but lacks ridges. The Candidate Research Location, found approximately 150 km at 110° (32.575439, -78.605161) east of Charleston, South Carolina, extends out as a finger from the inner/mid shelf transition with slopes as great as 10° and depth changes of 250 m or greater. Based on these criteria, the third location was identified as the candidate research location. Figures 10 and 11 show high-level views of the total DEM and the Candidate Research Location identified from the perspective of elevation and then slope.

Applying the same trigonometric equation used to verify the Currituck slope data, the arctangent was again used to calculate the approximate slope of the Candidate Research Location. The results were as expected for terrain bathymetry of the mid shelf. Measurements were taken at several different parts of the slump, calculating descent depth over distance of initial acceleration. At the steepest face, the slope measured 5° to 6°, whereas most other parts of the slope averaged 4° to 5° degrees. In four locations on the northern portion of the site, slopes were greater than 10° but exhibited little difference from top to bottom; they were not indicated on the elevation map as being different in their depth from surrounding areas. These values were crosschecked by running cell statistics from the ArcGIS Toolbox over the extent of the Candidate Research Location, deriving a 6.2° mean. It is important to recognize that the 87 m resolution DEM could be hiding steeper parts of the slump by generalizing areas.

The next step was to use these calculated data points to approximate the surface wave amplitude of a potential tsunami. The following method was applied to the overall difference of the Currituck slide and the Candidate Research Location. The calculated difference was used to determine the instantaneous surface elevation and the wave amplitude that would travel to the impact region. Since the slope values are stated as ranges per Prior et al., (1986) and again by Locat et al., (2009), calculating the differences as percentages was an effective method for arriving at an approximate total difference between the two cases. Table 1 shows the values used to arrive at the final outcome. All low and high values from the Candidate Research Location were calculated

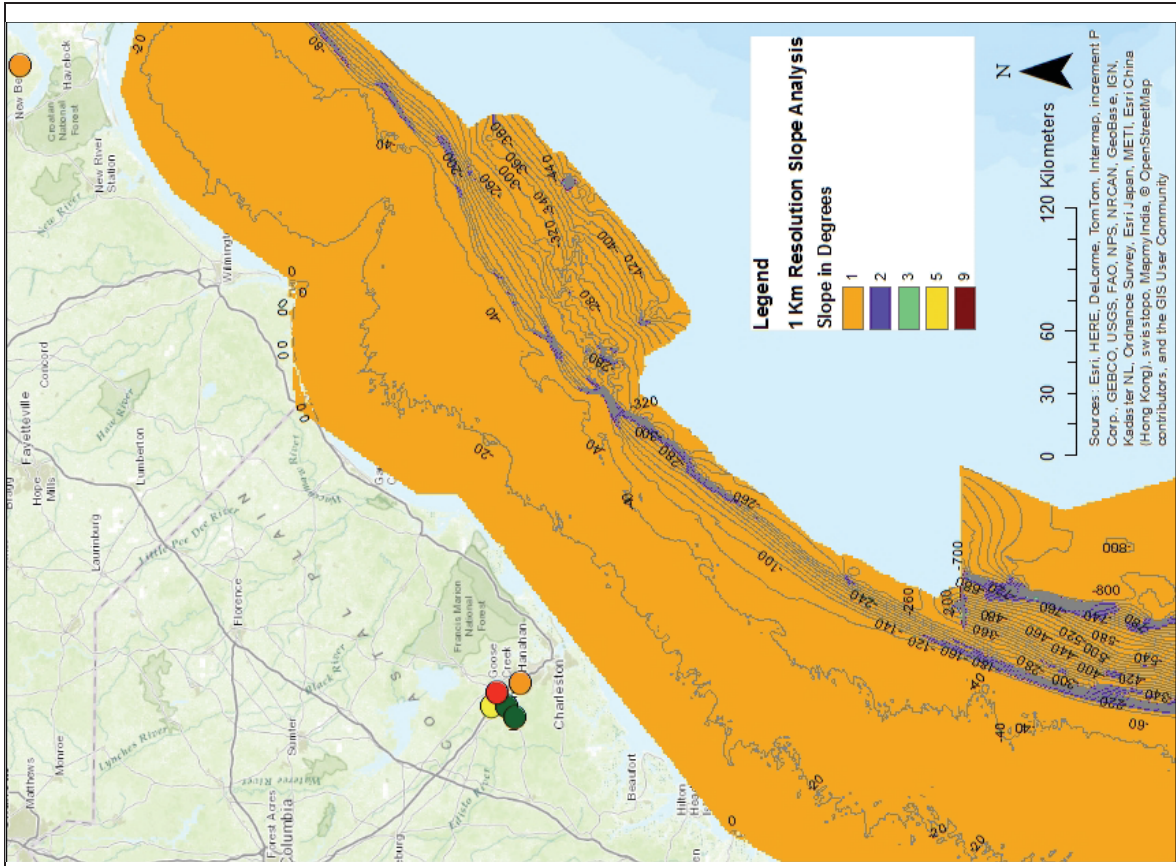
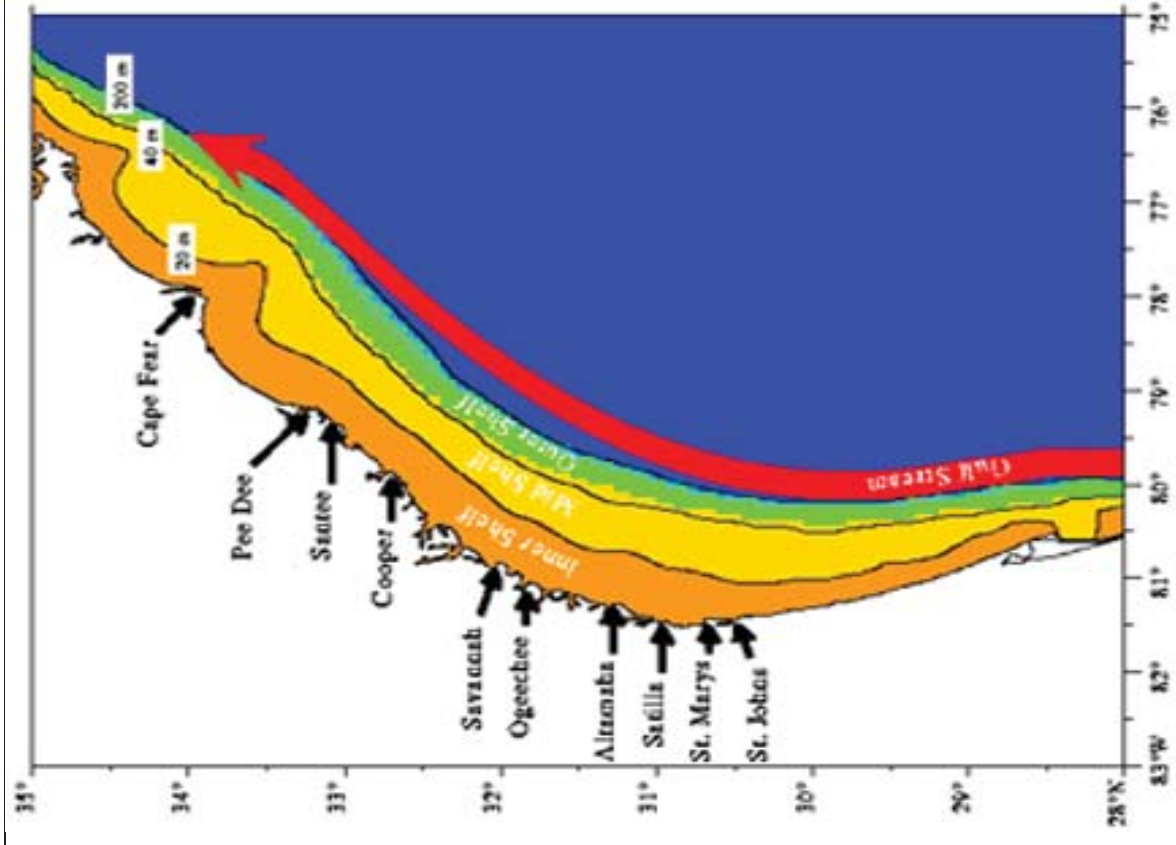


Figure 9. Distribution of continental shelf layers: Orange = Inner, Yellow = Mid, Green = Outer⁵ (left); Slope analysis of the inner and mid continental shelf for the southeastern U.S (right; resolution resampled at 1 km for better recognition).

against the low and high values for the upper and lower escarpments. For the Candidate Research Location, 5° and 6° represent the low and high averages of the area that exhibits the most potential for failure.

Table 1. Slope differences between candidate location and Currituck slide. All values relative to slope.

Candidate	Currituck	Difference	Sub-Averages	Cumulative Average
	Escarp-1			
5	9	-44%		
6	9	-33%	-42%	
5	10	-50%		
6	10	-40%		-58%
	Escarp-2			
5	15	-67%		
6	15	-67%	-73%	
5	30	-80%		
6	30	-80%		

Measuring 58% less in average cumulative descent slope over the entire research site, the Candidate Research Location would create approximately an instantaneous surface elevation of 11.52 m (37.80 ft) and a surface amplitude wave (tsunami) of 2.68 m (8.35 ft). Since the wave’s amplitude is measured peak to trough (top to bottom), the total amplitude is divided in half resulting in an above-surface height of 1.3 m (4.17 ft).

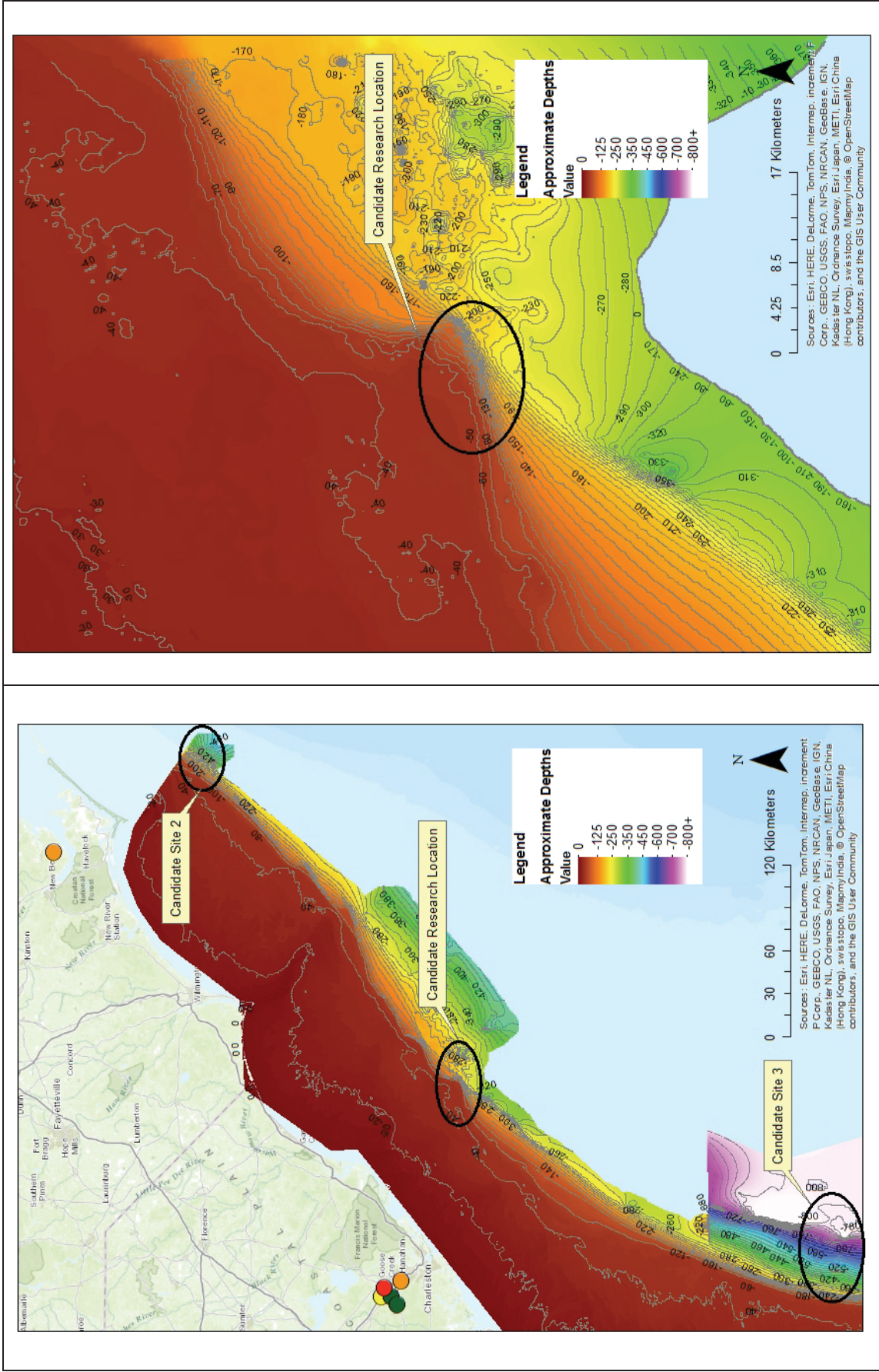


Figure 10. Southeast depth model for candidate research location identification.

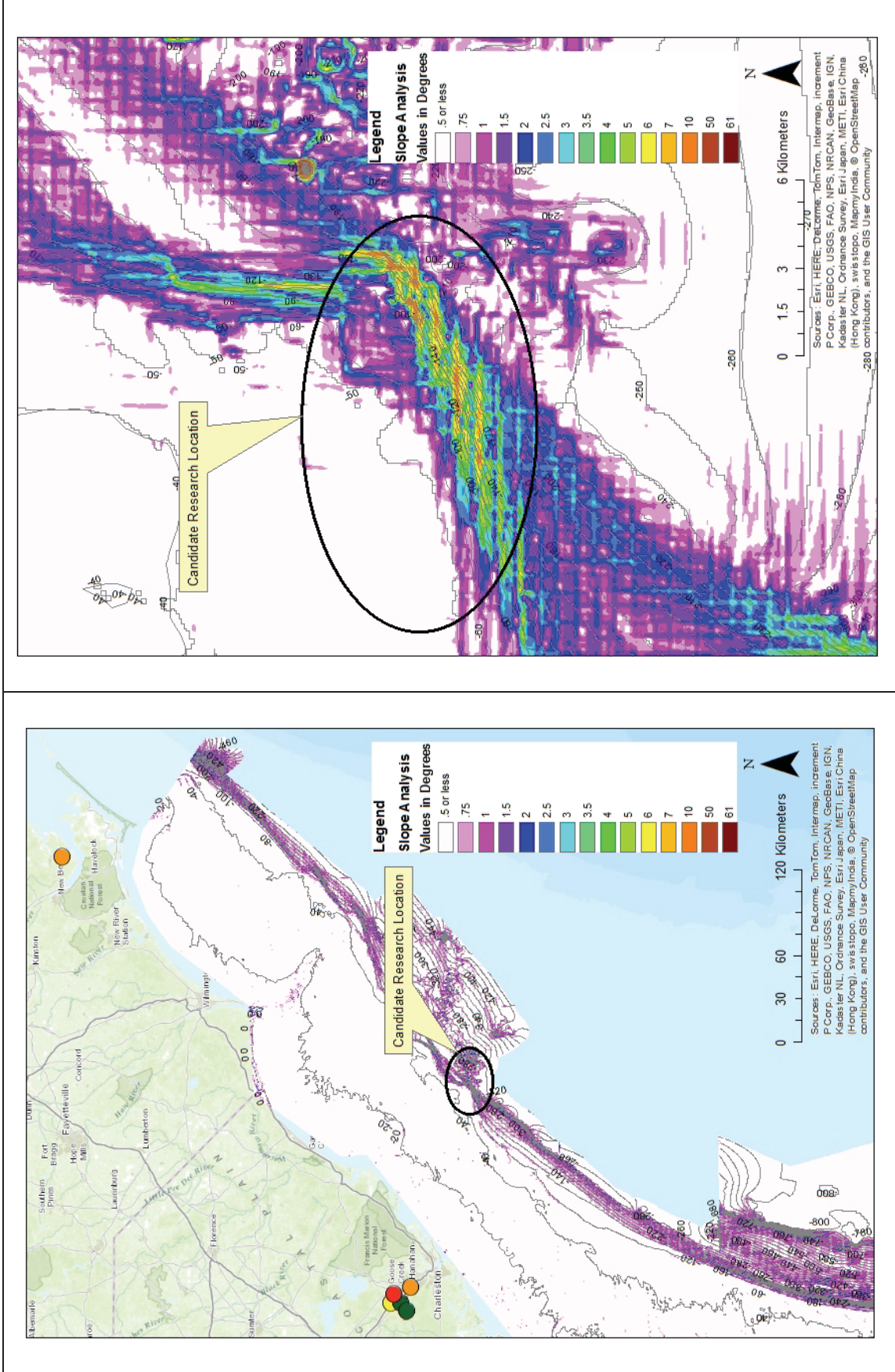


Figure 11. Southeast slope model for candidate research location identification.

Phase 3 – Tsunami Wave Propagation Modeling

GIS Least Cost and Buffer Method for Wave Impact Location Identification

Numerical models used for wave propagation are effective for computing many variables regarding the submarine terrain features and the velocity of sub-surface and surface waves. Although computing these parameters in a GIS would be possible, it would be an extraordinarily challenging task due to the complexity of formulas and equations needed to ensure consistent conclusions. As a substitute for numerical models, two common GIS functions were used to identify the first populated coastal region to be impacted by a tsunami generated at the Candidate Research Location and then to pinpoint what areas in that region would be struck first.

Buffers are used for a variety of tasks in GIS, such as identifying features within the proximity of a specific location. To identify the first populated location, buffers known as range rings were created from the center point of the Candidate Research Location extending in all directions at increments of 1 km and ending at 15 km (Figure 12). Since the precise angle for failure of the candidate site was unknown, even after performing an aspect analysis to determine the direction in which the slump faced, the azimuths for the two waves were unknown. Therefore, the range rings were used to project the wave propagation in all directions. Note that range rings resemble the wave expansion modeled by Grilli et al. (2015) using the FNW method for wave propagation.

The range rings show that waves propagating from the Candidate Research Location first make landfall on the coastal regions of the Francis Marion National Forest, north of Charleston. South of the national forest, the Isle of Palms, an island that is part of the City of Charleston, is the first populated impact location and is therefore the focus of the impact analysis discussed below. The Isle of Palms consists of northern and southern parts separated by a bridge. Because the northern part is the first affected by the wave and because of the modeling requirements, the northern part was used for the impact modeling and analysis.

Another GIS method for calculating the likelihood of where a wave may make landfall is to use a least cost analysis function to plot a route based on a cost surface raster. The least cost path analysis consists of reclassifying a surface, either vector or raster, by a cost factor. Many least cost paths are calculated using slope or elevation rasters. Reclassification can be unsupervised or supervised, where ranges or values are entered manually and assigned a cost. The range of costs is constructed with a relatively low number, such as 1, representing the lowest cost, and some number greater than the lowest cost, such as 10, being the highest cost. Costs are then proportionally spread across a range, representing costs that lie somewhere between the lower and upper limits. In performing a least cost path analysis, each raster cell or pixel is assigned a value. When a path is calculated, the placement of the next cell in the path is based on the independent cost of neighbor cells, where the value of lowest cost will be the next addition.

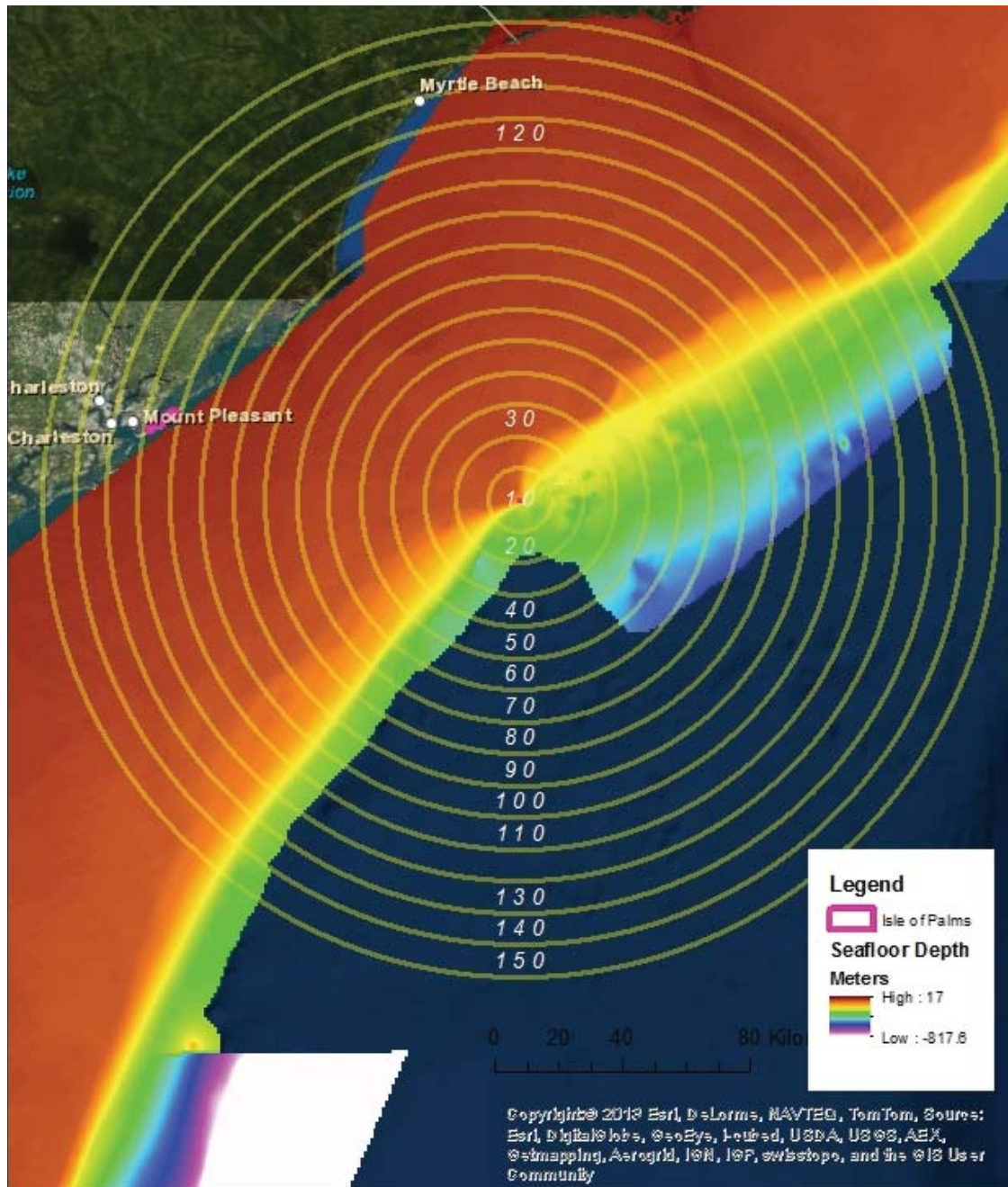


Figure 12. Range rings identifying impact location, assuming equal propagation from candidate research location.

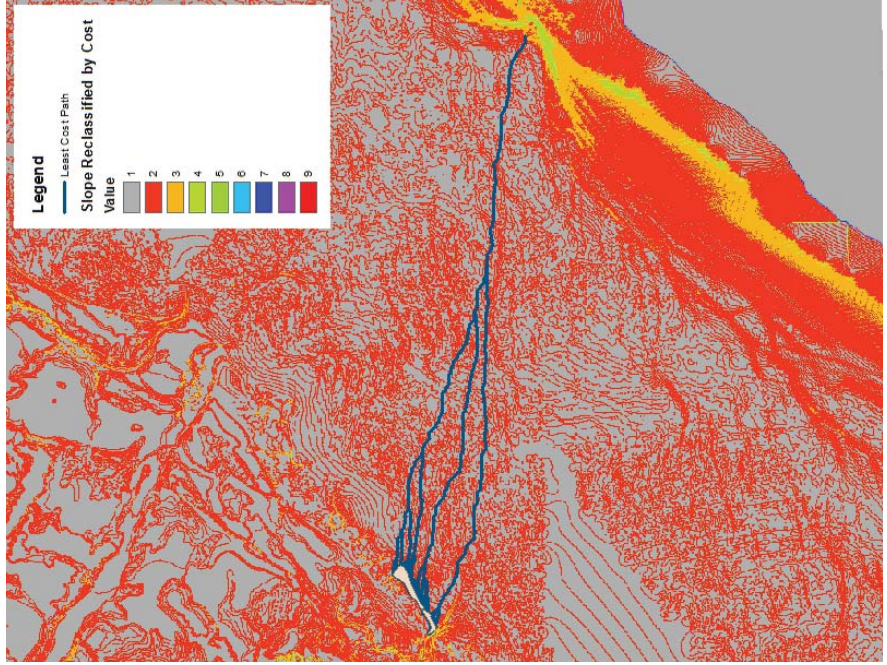
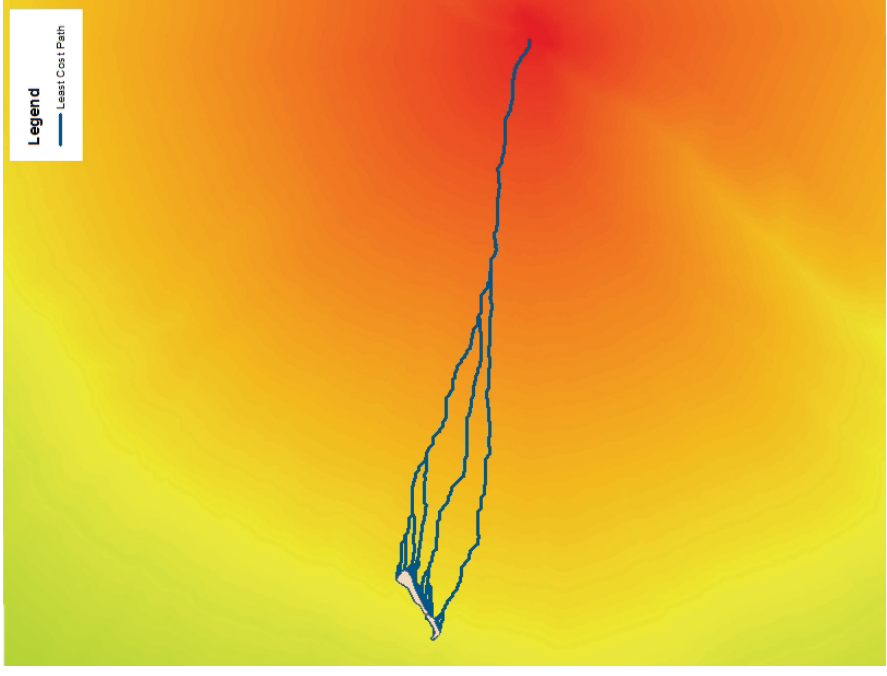
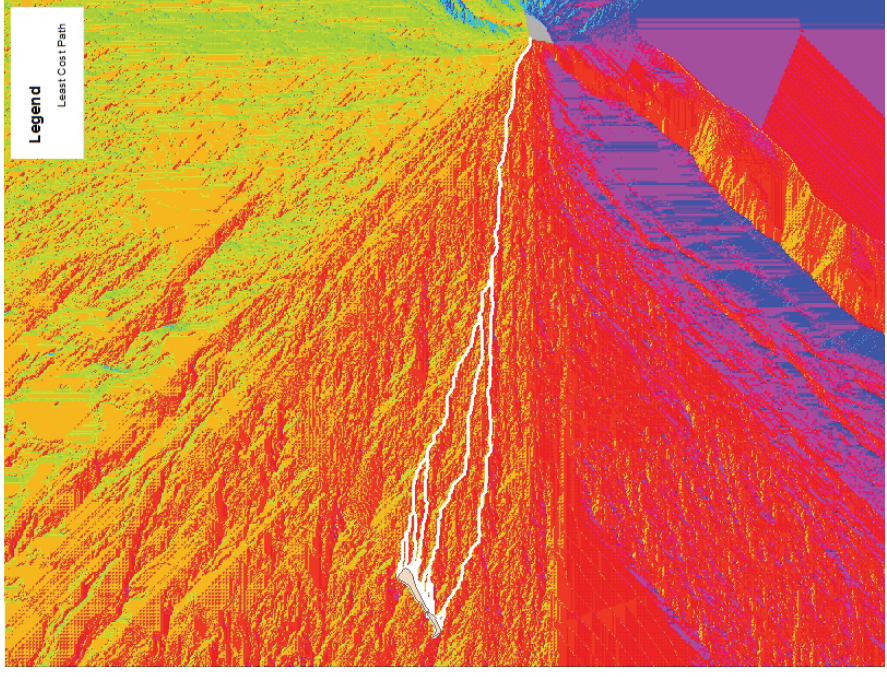


Figure 13. Reclassified slope analysis by cost (left), cost distance (middle), backlink analysis (right).

Figure 13 shows the three outputs resulting from the least cost analysis. The left-hand graphic represents the reclassified 87 m resolution slope raster, with nine classes used to classify the image. Greater gradients were classified as higher costs while lower gradients were cheaper in cost. In the center graphic, a cost surface shows expanding surface cost from the source location, the candidate landslide, to the destination, the Isle of Palms. In this case, cheaper costs are calculated relative to the increased distance from the Candidate Research Location. In the right-hand graphic, a backlink analysis associates pixels with a cardinal direction (N, NE, E, SE, S, SW, W, NW). The analysis takes both the reclassified surface raster and the cost surface into account when creating the backlink. A cost path is the final step in the process, which draws upon the backlink, source, and destination layers to plot a route from lowest costing pixel to the next least costly pixel before terminating at the destination.

All three graphics display the resulting least cost path to the Isle of Palms. Typically, a point-to-point cost path would be calculated. In this analysis, two polygons were used, resulting in the multi-line arrangement between the two locations. When the shortest path was measured, it was discovered that the northeastern part of the island would be the first to be impacted by a tsunami generated at the Candidate Research Location.

Tsunami Inundation Impact Model

To develop the tsunami inundation impact model, a DEM and height-accurate building structures were created for most of the northern portion of Isle of Palms by using light detection and ranging (LIDAR) data collected by NOAA for ground return and USGS for all returns. A building layer was obtained from the Charleston City Government for residential and commercial building footprints. Additional .5 m high-resolution orthorectified imagery was obtained from USGS. All imagery layers were consolidated in ESRI ArcScene for three-dimensional modeling. The building footprint layer was interpolated from the Z-max values of the all-return LIDAR point cloud.

Using the Clack Hydrology Flood Model, discussed in Phase 4, an output polygon layer was extruded using the calculated tsunami surface wave height of 1.3 m to match the wave-height and simulate inundation on the island, extending inward from the first point of contact in the northeast. The model shows initial contact but does not go so far as to show the effects of waves crashing on themselves and building volume. Figure 14 shows a screen shot of this model.⁶

⁶ Visit [Isle of Palms Tsunami Impact](#) for a user-driven 3D fly through experience.



Figure 14. Representation of wave impact on Isle of Palms; color values according to Z-height.

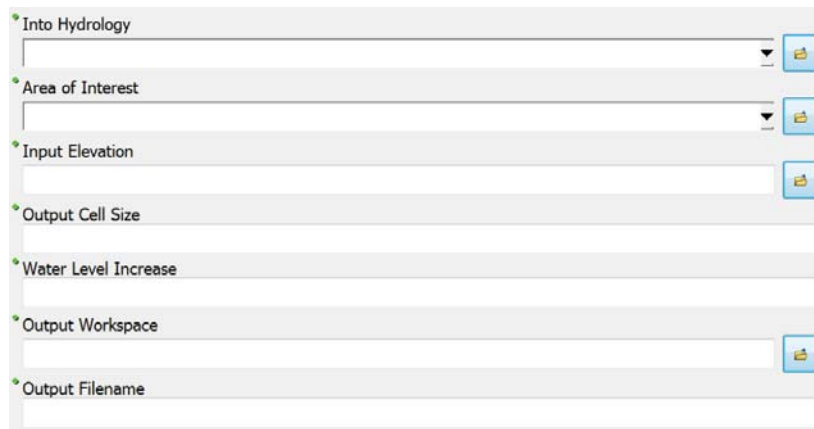
Phase 4 – Wave Inundation Impact Analysis

Two terrain models were built to simulate inundation effects from a tsunami surface wave. Original expectations of the impact analysis assumed major impacts on lines of communication, residential and commercial areas, and key infrastructure locations such as power plants and ports. These assumptions were based on the findings from the Currituck SMF tsunami and its surface wave of 3–6 m in amplitude. However, the results based on the method used with the Candidate Research Location created a far less powerful wave with minimal effects on the Isle of Palms. Since the surface wave was calculated to be only 1.3 m (4.3 ft) above mean sea level (MSL), natural barriers of the island provided sufficient protection from the hypothetical tsunami.

Two methods, a difference model and a method developed by a colleague, Alan Clack, which will be referred to as the Clack Hydrology Flood Model (or Clack model, for short), were used to create maps showing the effects of the surface wave’s inundation of the island. For both models, an additional meter was added to the surface wave to account for the fact that the LIDAR used to create the DEM was collected during low tide and an approximately 1-m difference was measured to the MSL at high tide. This inundation is therefore still representative of a 1.3 m surface wave.

The difference model is a straightforward approach for identifying parts of the island where elevations are equal to or lower than the height of the surface wave. This was done by using a map algebraic equation to create a new raster from the DEM, highlighting areas with an elevation equal to or less than 1.3 m. The new raster was reclassified to show only areas that meet the function.

The Clack model uses a more sophisticated approach that includes a gravitational motion effect. It is an exclusively GIS spatial model developed to create sufficiently accurate flood predictions without having to use expensive and highly customized software. One main difference from the difference model is how the Clack model simulates the flow of water according to the surface elevation. Figure 15 displays the script user interface with required fields.



The image shows a script user interface for the Clack model. It consists of several input fields, each with a small blue icon to its right. The fields are: 'Into Hydrology' (a dropdown menu), 'Area of Interest' (a dropdown menu), 'Input Elevation' (a text input field), 'Output Cell Size' (a text input field), 'Water Level Increase' (a text input field), 'Output Workspace' (a text input field), and 'Output Filename' (a text input field).

Figure 15. Clack model script user interface.

The three input layers from Figure 15 required to run the model are the input hydrology (Layer A), the area of interest (Layer C), and the input elevation (Layer B). Figure 16 identifies each of the three layers with layer notation, which are referenced in the sequential processing steps. In addition to the three layers, two additional layers are discussed in the processing steps. They include multipoint vectors that to which the DEM is converted; and the Triangulated Irregular Network (TIN), which is an accurate method for the representation of terrain by calculating small various-sized triangles across the surface area, where the vertices connect to points. The processing steps are as follows:

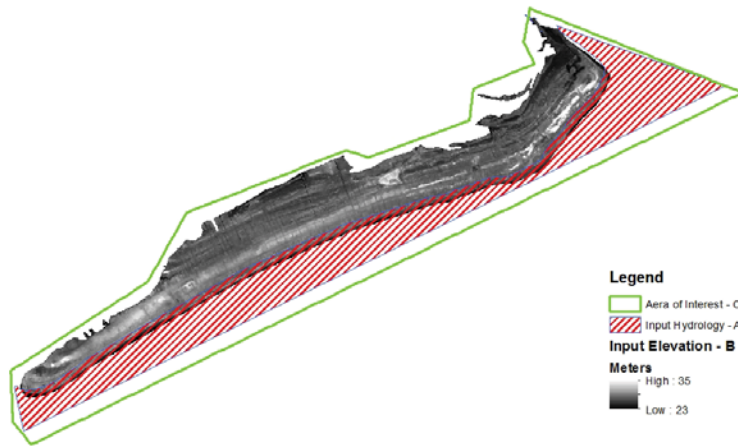


Figure 16. Clack model input layers.

1. The layer B DEM is converted to a multipoint layer (Figure 17).

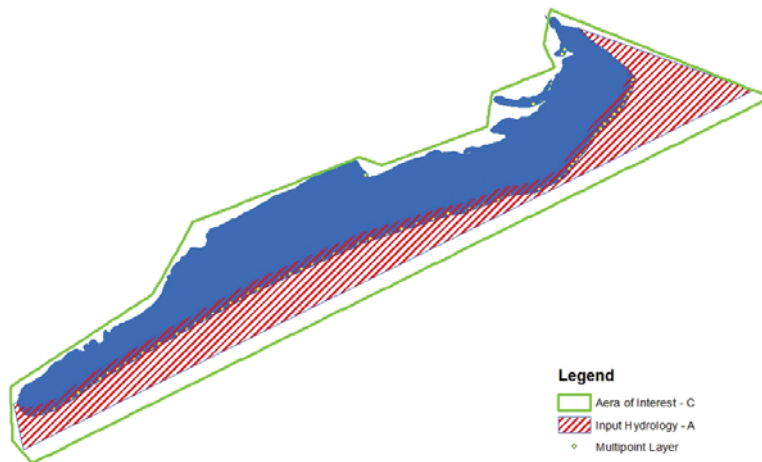


Figure 17. DEM to multipoint (blue layer).

2. The layer A input hydrology, which acts as the wave or flooding layer, is converted from a polygon to a raster, then from a raster to a TIN (Figure 18).

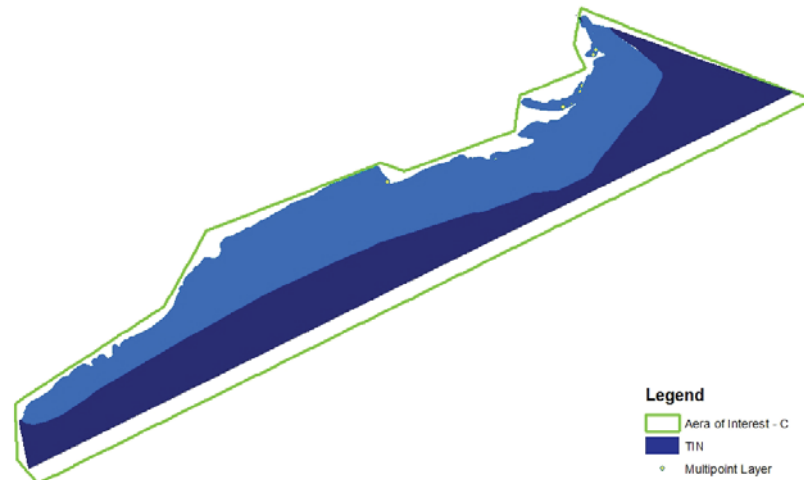


Figure 18. Hydrology raster to TIN.

3. Layer C is then used as the extraction extent from which excess boundaries are eliminated, or clipped, to reduce the number of unnecessary calculations outside of the area of interest.
4. The surface wave height is added to the hydrology layer using map algebra.
5. The gravitational effect is applied as the layer A TIN vertices are snapped to the layer C points using layer C as the processing extent. The original TIN created from step 2 expands to encapsulate the multipoint layer and then is converted to a raster (Figure 19).

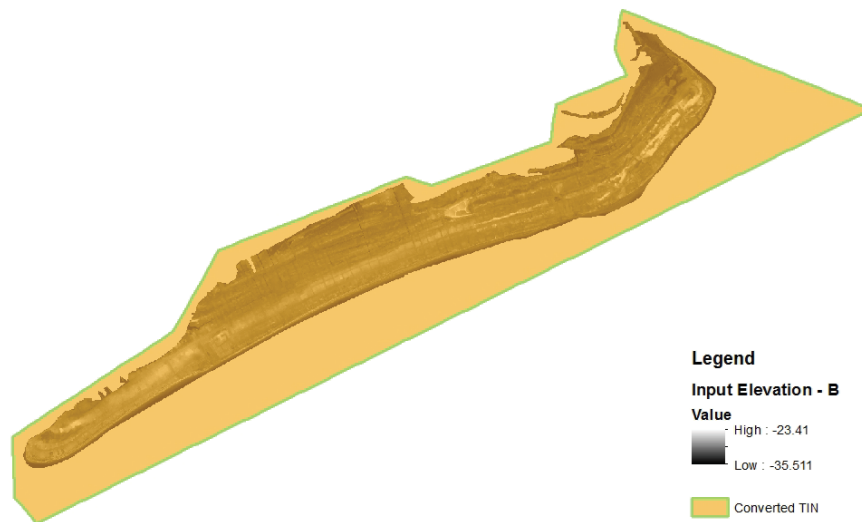


Figure 19. Snapped TIN to multipoint.

6. The original layer B DEM is subtracted from Layer A (Figure 20). All resulting values less than or equal to (0) are interpreted as no flooding. Anything greater is represented as a flood raster.

Step 5 is the point at which the Clack model differs from the difference method in that, in this model, there comes a point at which the wave no longer has the height needed to move further toward the boundary of the area of interest. Figure 21 is the final output of the Clack model.

Legend

Adjusted Wave Inundation



Figure 20. Difference Model for DEM ≤ 1.3 m.

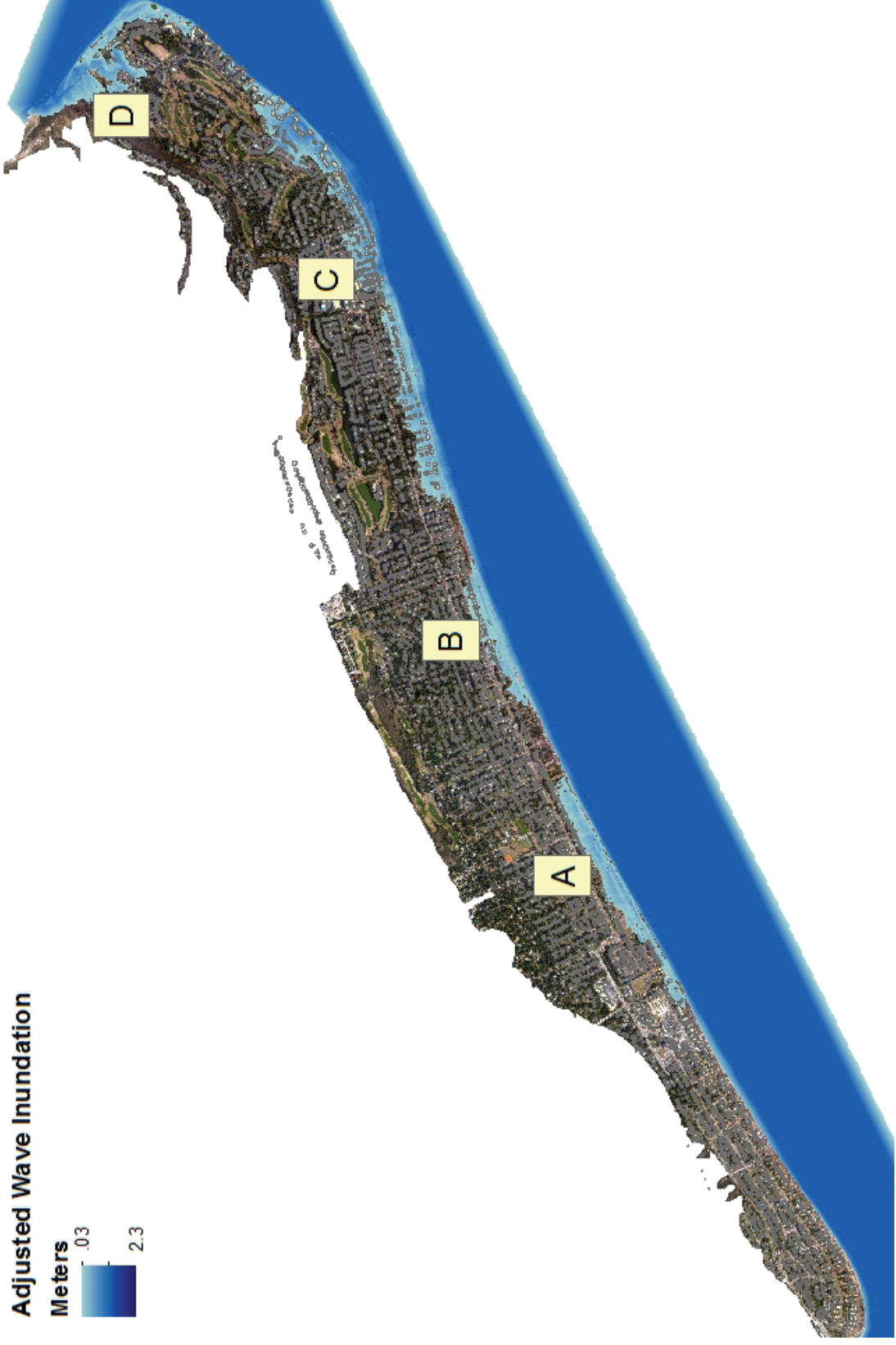


Figure 21. Clack model; the letters correspond to the site-specific inundation zones shown in Figure 22.

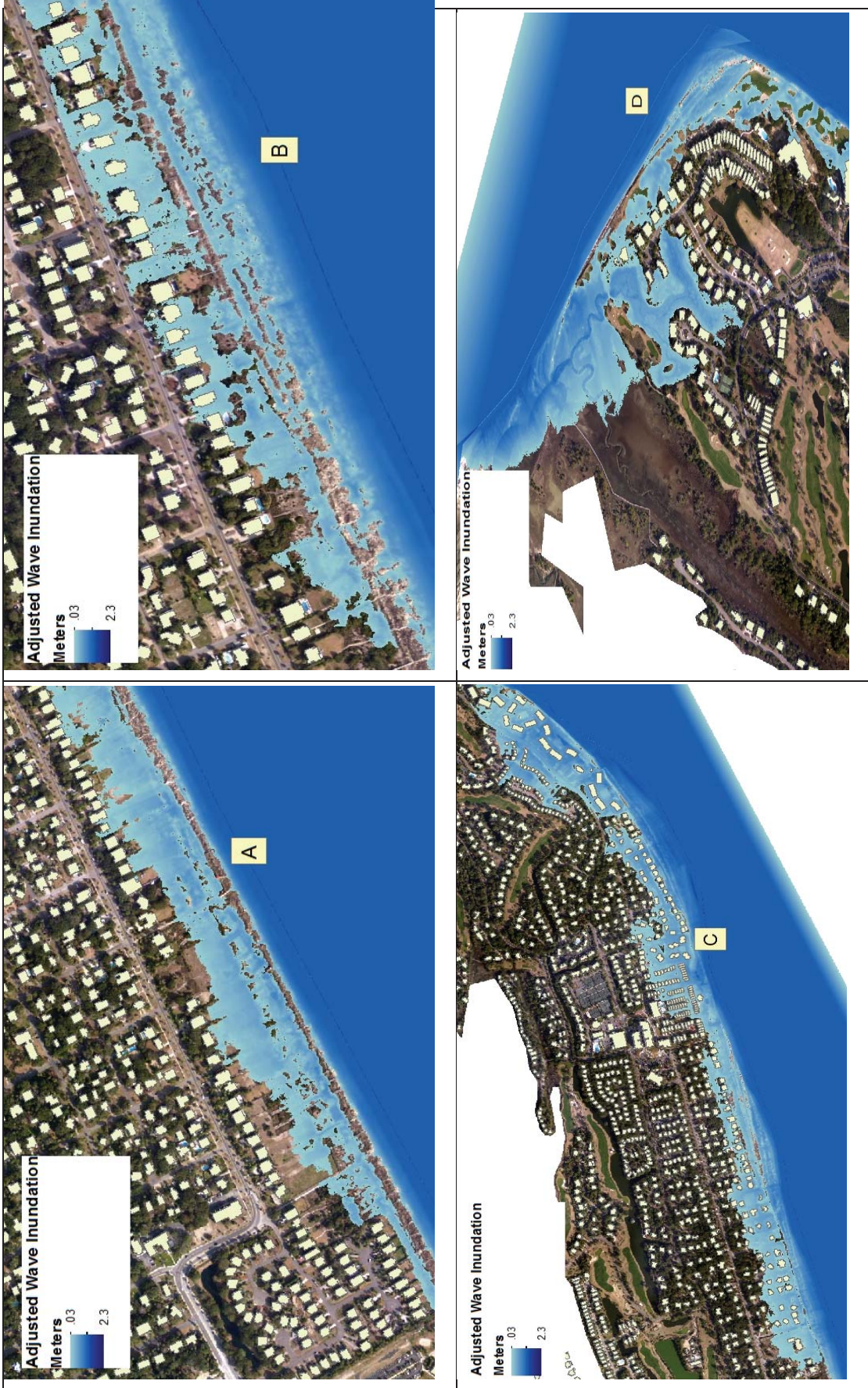


Figure 22. Site-specific inundation locations.

Results

The difference method finds that flooding from the surface wave results in minimal impacts to the eastern coast of the island (Figure 20). Penetration of the dunes occurs in the northeast but has no impact because the floodwaters dissipate over the sand and so do not reach any housing and dissipates over the sand. The model suggests that flooding on the western side of the island is more substantial, but these findings are ignored due to how the difference method works, i.e., areas identified as being flooded are swaths of ground with elevations equal to or lower than the height of the surface wave. The northern tip of the island does show flooding over the marshlands, parts of a golf course, and one neighborhood. The degree of flooding cannot be interpreted from the difference model output, however, because the model can demonstrate only that the terrain is at risk of flooding based on the DEM height.

The Clack Model output (Figure 21) identifies four locations that were susceptible to flooding (Figure 22). These locations include three on the eastern coast (sites A, B, and C) and the same area to the north that the difference approach revealed would be at minor risk (site D). Sites A and B are flooded by between 0.10 m (4 in) and 0.15 m (6 in) of water. Most of the homes along the coasts are built on stilts, so they are at minimal risk of flooding. Site C is the highest risk, with water heights ranging from 0.1 m (4 in) to over 1.2 m (4 ft). One community in the northeastern part of Site C is the most affected area. Site C has many tall structures rather than of single-family homes, which could account for lower surface terrain due to the larger building's footprints requiring ground leveling over a large area. In this region, several roads would be covered in water and most vehicles would be immobilized. The eastern areas of Site D are the first to come in contact with the wave but are also largely protected, as the dunes at that location are the most built up. Some flooding does surpass the barrier but little water actually makes contact with the hotel and residential properties. The northern tip of D experiences similar inundation as found in the difference method; however, water does not penetrate inward towards the island to nearly so great an extent. This is because the difference model does not account for surface elevation variances. This variance can be seen in and around the residential properties and the marsh regions. Fewer than five properties come in contact with the wave itself, with most of the inundation occurring in roadways lower than property plots.

Conclusions

This paper was written with the objective of applying an exclusively GIS-based approach for identifying regions susceptible to an earthquake-produced landslides and coastal areas susceptible to a tsunami surface wave. The study included a four-phase approach covering a statistical earthquake data analysis, topographic seafloor analysis for a candidate site selection, wave propagation modeling, and an impact analysis on the Isle of Palms, South Carolina.

In Phase 1, earthquake epicenter densities were measured using point data to assess what locations, over the past 25 years and within 100 km of the U.S. East Coast, were the most active. The densest cluster of seismic events took place in the vicinity of Charleston South Carolina. The Phase 2 seafloor analysis was performed off the coasts of South

Carolina, northern Georgia, and southern North Carolina and involved determining slope and elevation similarities to the historic Currituck SMF in order to gauge both site suitability and energy output. Due to bathymetric data availability in the U.S. Southeast, analysis was conducted of the inner and mid-continental shelves only, and revealed a very gradual slope descent with few locations that offered characteristics similar to known submarine failures.

In Phase 3, using the Currituck SMF characteristics, a comparison was performed on the selected candidate location revealing a 58% difference in overall steepness. Since the main SMF factor in tsunami generation is the initial downward acceleration, a 58% difference was applied to both the candidate location instantaneous wave surface height and the tsunami amplitude. A least cost path analysis and buffers were used to identify the first populated area in the wake of the tsunami.

In Phase 4, an impact analysis was conducted on the Isle of Palms South Carolina applying two separate methods in determining flood inundation from a tsunami surface wave. Use of a simple difference method accounted only for terrain with an elevation of less than the height of the wave, while a more sophisticated approach, the Clack Model, considered both terrain and wave elevation relative to one another in predicting potential inundation.

These results are based solely on available data and do not rule out the possibility of more substantial impacts from larger SMF-induced tsunamis.

The overall process of performing statistical point data analysis, seafloor analysis, landslide and tsunami characterization, modeling, and impact analysis could serve as a prototype for assessing tsunami risk through the exclusive use of Geographic Information Systems. This paper does not contend that GIS are in all ways better alternatives to specialized numerical models, as those models capture and articulate precise calculations at a granular scale. Nonetheless, GIS do offer a way to arrive at similar conclusions by using tools and methods that are more accessible than those requiring specialized knowledge of marine geology, hydrodynamics, and geophysics. Moreover, few scientific papers or projects utilize GIS for applying historical data surrounding seismic activity or using spatial analytics to anticipate a probable zone of imminent danger from a tsunami. Research projects such as this one can help emergency planners prepare for the possible occurrence of tsunami, thereby potentially mitigating the impacts of tsunami by strengthening emergency preparedness and preserving property and life.

References

- Bardet, J.-P., C. E. Synolakis, H. L. Davies, F. Imamura, and E. A. Okal, 2003. Landslide Tsunami: Recent Findings and Research Directions. *Pure and Applied Geophysics*, 160: 1793-1809.
- Barker, G.C., Mehta, A., 1994. The Dynamics of Sand, *Reports on Progress in Physics*, 57 (4) pp. 383.
- City of Charleston GIS. <http://gis.charleston-sc.gov/dataportal/>
- Grilli, S., J. Harris, F. Shi, J. Kirby, T. Tajalli Bakhsh, E. Estivals, and B. Tehranirad, 2012. Numerical Modeling of Coastal Tsunami Impact Dissipation and Impact. *Coastal Engineering Proceedings*, 1 (33), 9 pp.
- Grilli, S., C. O'Reilly, J. Harris, T. Bakhsh, B. Tehranirad, S. Banihashemi, J. Kirby, C. Baxter, T. Eggeling, G. Ma, and F., Shi, 2015. Modeling of SMF Tsunami Hazard Along the Upper US East Coast: Detailed Impact around Ocean City, MD. *Natural Hazards*, 76 (20): 705-746.
- Harbitz, C. B., F. Løvholt, and H. Bungum, 2014. Submarine Landslide tsunami: How Extreme and How Likely? *Natural Hazards* 72 (3):1341-1374.
- Harris, J., S. Grilli, S. Abadie, T. Bakhsh, . Near- and Far-field Tsunami Hazard from the Potential Flank Collapse of the Cumbre Vieja Volcano, 2012. *Proceedings of the Twenty-second (2012) International Offshore and Polar Engineering Conference*, Rhodes, Greece, June 17–22, pp. 242-249.
- Heidarzadeh, M., K. Satake, S. Murotani, A. Gusman, and S. Watada, 2015. Deep-Water Characteristics of the Trans-Pacific Tsunami from the 1 April 2014 Mw 8.2 Iquique, Chile Earthquake. *Pure and Applied Geophysics*, 172 (3-4): 719-730.
- Iacono, C. L., E. Gracia, F. Zaniboni, G. Pagnoni, S. Tinti, R. Bartolome, D. Masson, R. Wynn, Nuno. Lourenco, M. Pinto de Abreu, J. Danobeitia, and V. Zitellini, 2012. Larger, Deepwater Slope Failures: Implication for Landside-Generated Tsunamis. *Geological Society of America* 40 (10): 931-934.
- Kirby, J.T.a, Shi, Fengyan a, Tehranirad, Babak a, Harris, Jaffrey C. b, Grilli, Stephan T. b, (2013). Dispersive tsunami waves in the ocean: Model equations and sensitivity to dispersion and Coriolis effects. a Center for Applied Coastal Research, University of Delaware & b Department of Ocean Engineering, University of Rhode Island. *Elsevier: Ocean Modeling*, 62 (2013): 39-55.
- Landslide Types and Processes, 2004. U.S. Dept. of the Interior & U.S. Geologic Survey. Fact Sheet 2004-3072. <http://pubs.usgs.gov/fs/2004/3072/fs-2004-3072.html>

L'Heureux, J.-S., A. Locat, S. Lerouil, D. Demers, and J. Locat, 2013. Landslides in Sensitive Clays – From Geosciences to Risk Management. In: *Landslides in Sensitive Clays – From Geosciences to Risk Management*, J.-S. L'Heureux, A. Locat, S. Lerouil, D. Demers, and J. Locat (Editors), Springer Netherlands, pp. 1-12.

Liu, P. L., H. H. Yeh, and C. Synolakis, 2008. *Advanced Numerical Models for Simulation Tsunami Waves and Run-Up*. [Advances in Coastal and Ocean Engineering](#), Volume 10. Hackensack, N.J. and London: World Scientific.

Locat, Jacques, Lee, Homa, ten Brink, Uri S., Twichell, David, Geist, Eric, and Sansoucy, Mylene, 2008. Geomorphology, stability and mobility of the Currituck slide. *Marine Geology*, Elsevier, Volume 264 (2009): 28 – 40.

Ma, G., Shi, F., Kirby, JT, 2012. Shock-capturing non-hydrostatic model for fully dispersive surface wave processes. *Ocean Modeling*, 43–44 (2012): 22–35.

Mehta, A., Barker, G. C., 1994. The Dynamics of Sand. *Reports on Progress in Physics*, 57 (4): 383 – 416.

[National Tsunami Hazard Mitigation Program History 1995 – 2005](#). National Oceanic and Atmospheric Administration.

Office of Naval Research, Science, and Technology. Outer Continental Shelf. <http://www.virginiaplaces.org/boundaries/ocs.html>

Park, H., D. Cox, and C. Petroff, 2015. An Empirical Solution for Tsunami Run-Up on Compound Slopes. *Natural Hazards*, 76 (3): 1727-1743.

Parry, Wynne, 2011. What's the Science Behind Japan's Earthquake and Tsunami?. http://www.livescience.com/13187-japan-earthquake-tsunami-science-faq.html?li_source=pm&li_medium=more-from-livescience&li_campaign=related_test

Prior, David B., Dyle, Earl H., and Neurauter, Tom, 1986. The Currituck Slide, Mid-Atlantic Continental Slope – Revisited. *Marine Geology*, Elsevier, Volume 73 (1986): 25 – 45.

Sammarco, P., and E. Renzi, 2008. Landslide Tsunamis Propagating along a Plane Beach. *Journal of Fluid Mechanics*, 598:107-119.

South Carolina Department of Natural Resources Charleston County Lidar – 2009, 2014. National Oceanic and Atmospheric Administration. <https://data.noaa.gov/dataset/2009-scdnr-charleston-county-lidar>.

South Carolina Department of Transportation, 2015. <http://info.scdot.org/sites/GIS/SitePages/GISFiles.aspx?MapType=Warehouse>

South Carolina Geographic Information Systems, 2008.
<http://www.gis.sc.gov/data.html#Commerce> .

Tinti, S., and R. Tonini, 2005. Analytical Evolution of Tsunamis Induced by Near-Shore Earthquakes on a Constant-Slope Ocean. *Journal of Fluid Mechanics*, 535: 33-64.

Tsay, T., Liu, P., and Wu, N, 2001. A Nonlinear Model for Wave Propagation. [Coastal Engineering Proceedings](#), 1(25): 589-601.

United States Geologic Survey (USGS). Earthquake Hazards Program.
<http://earthquake.usgs.gov>.

Zhao, X., B.L., and H. Liu, 2009. Numerical Simulations of Tsunami Generation by using Boussinesq Equations. In: *New Trends in Fluid Mechanics Research*, F. G. Zhuang and J. C. Li (Editors), Springer Berlin Heidelberg, pp. 411.